RESEARCH PAPER

"Quality-by-Design Based Development and Optimization of Ciclopirox Olamine-Loaded Transethosomes for the Treatment of Fungal Infections"

Nasheer Shaikh*, Karbhari Vaishnavi[1], Bharti Ashwini, Khune Mayuri, Akkangire Bhagyashri, Bhaidode Manjunath
Dept. of Pharmaceutics, Channabasweshwar Pharmacy College (Degree), Near Basweshwar Chowk, Kava Road, Latur-413512 (MS)
***Corresponding Author: Dr. Shaikh Nasheer S.**
*Associate Professor & Head, Dept. of Pharmaceutics, Channabasweshwar Pharmacy College (Degree), Near Basweshwar Chowk, Kava Road, Latur-413512 (MS), nasheershaikh@gmail.com

ABSTRACT

Background: Cutaneous fungal infections are highly prevalent and frequently recurrent, yet conventional topical antifungals penetrate the stratum corneum poorly, limiting cure rates. Ciclopirox olamine (CPO), a broad-spectrum hydroxypyridinone antifungal acting by chelation of polyvalent metal cations, is limited by low aqueous solubility and poor skin penetration. Transethosomes ultradeformable vesicles combining ethanol and an edge activator were investigated to overcome these limitations.

Methods: CPO-loaded transethosomes were prepared by the cold method and optimized using a three-factor, three-level Box–Behnken design (soya lecithin, ethanol, Tween 80) for particle size, drug content and entrapment efficiency. The optimized batch (Trans-01) was characterized by DLS, zeta potential, SEM, XRD and FTIR, incorporated into a Carbopol 934 bioadhesive gel, and evaluated for in-vitro release, ex-vivo permeation, antifungal activity against Trichophyton rubrum, and stability.

Results: Trans-01 showed a particle size of 112.3 nm, PDI 0.353, zeta potential 29.7 mV, drug content 90.2% and entrapment efficiency 92.5%. XRD confirmed drug amorphization within the bilayer. The gel achieved 66% ex-vivo permeation over 24 h, a 14 mm zone of inhibition (70% of the miconazole standard), and remained physically and chemically stable under ICH accelerated conditions.

Conclusion: A quality-by-design optimized CPO transethosomal bioadhesive gel provides enhanced, sustained topical antifungal delivery and represents a promising candidate for treating dermatophytic skin infections.

How to cite this article: Nasheer Shaikh* Karbhari Vaishnavi1 Bharti Ashwini Khune Mayuri Akkangire Bhagyashri Bhaidode Manjunath. "Quality-by-Design Based Development and Optimization of Ciclopirox Olamine-Loaded Transethosomes for the Treatment of Fungal Infections". Int J Drug Deliv Technol. 2026;16(82s):789-796. DOI: 10.25258/ijddt.16.82s.89.

1. INTRODUCTION

Transethosomes are a novel class of ultradeformable vesicular nanocarriers that combine the penetration-enhancing features of both ethosomes and transfersomes for topical and transdermal drug delivery. They are lipid-based colloidal vesicles composed of phospholipids, a relatively high concentration of ethanol (20–45% v/v) and at least one edge activator (a surfactant such as Tween 80, Span 80 or sodium deoxycholate). This architecture gives the vesicles exceptional membrane elasticity and the ability to squeeze through the stratum corneum without losing integrity, providing skin-penetration enhancement that surpasses either parent system used alone.

The rationale for transethosomes arises from the limitations of conventional vesicles. Classical liposomes have rigid bilayers and penetrate the skin poorly; ethosomes added ethanol to fluidize stratum-corneum lipids but lack mechanical deformability; transfersomes added edge activators for elasticity but lack alcoholic lipid fluidization. Transethosomes combine both mechanisms, markedly amplifying dermal bioavailability. Phospholipids form the vesicular bilayer, ethanol fluidizes both vesicle and skin lipids, and the edge activator lowers bilayer rigidity to confer ultradeformability.

Cutaneous fungal infections dermatophytosis (caused mainly by Trichophyton, Microsporum and Epidermophyton species), cutaneous candidiasis and superficial mycoses such as tinea versicolor affect an estimated 20–25% of the world population and are prone to chronicity and relapse. Their pharmacotherapy relies largely on topical azoles and allylamines, but treatment success for chronic, recurrent or nail-involving infections remains suboptimal because insufficient drug reaches the fungal niche within the epidermis and upper dermis.

Ciclopirox olamine (CPO) was selected as the model drug. It is a broad-spectrum synthetic hydroxypyridinone antifungal that acts by chelating polyvalent metal cations (particularly Fe^{3+}), thereby inhibiting metal-dependent fungal enzymes essential for metabolism and membrane integrity. This mechanism is distinct from the azoles and confers activity against dermatophytes, Candida, Malassezia and several opportunistic moulds. However, its high lipophilicity and low aqueous solubility limit penetration into deeper skin layers from conventional creams and solutions, making it a strong candidate for vesicular delivery.

Incorporating CPO-loaded transethosomes into a Carbopol-based bioadhesive gel is expected to overcome these pharmacokinetic limitations: the deformable vesicles enhance penetration and drug deposition at the site of infection, while the bioadhesive polymer prolongs residence time and sustains release, maintaining drug levels above the minimum inhibitory concentration and supporting reduced dosing frequency and improved patient adherence. The present work therefore develops, optimizes and evaluates a CPO-loaded transethosomal bioadhesive gel for enhanced topical antifungal therapy.

2. NEED OF STUDY

- Cutaneous fungal infections affect millions worldwide and remain a major public-health concern due to frequent recurrence and incomplete treatment outcomes.
- Conventional topical antifungal formulations often fail to deliver sufficient drug to deeper skin layers, reducing therapeutic efficacy.
- Ciclopirox olamine exhibits poor aqueous solubility and high lipophilicity, which limit its skin permeation and availability at the infection site.
- The stratum corneum is a strong barrier restricting penetration of conventional creams and gels, and emerging antifungal resistance demands delivery systems achieving higher local drug concentrations.
- Poor skin retention of conventional formulations leads to frequent application and reduced patient compliance.
- Transethosomes possess enhanced deformability

and, through the combination of ethanol and edge activators, provide superior skin permeation compared with conventional liposomes and ethosomes.

- Incorporating transethosomes into a bioadhesive gel can prolong residence time and provide sustained release, improving antifungal efficacy and adherence.
- A ciclopirox olamine-loaded transethosomal bioadhesive gel thus addresses an important research gap and offers a promising strategy for effective topical antifungal therapy.

3. AIM AND OBJECTIVE

3.1 Aim

To develop and optimize a ciclopirox olamine-loaded transethosomal bioadhesive gel for enhanced topical delivery and treatment of fungal skin infections.

3.2 Objectives

- To perform preformulation studies of ciclopirox olamine and selected excipients, including physicochemical characterization and compatibility assessment.
- To formulate ciclopirox olamine-loaded transethosomal vesicles by the cold method and evaluate their physicochemical properties.
- To optimize the transethosomal formulation using a Box–Behnken design and design of experiments.
- To characterize the optimized transethosomes for vesicle size, PDI, zeta potential, morphology, XRD and entrapment efficiency.
- To incorporate the optimized transethosomes into a bioadhesive gel and evaluate its rheological and physicochemical properties.
- To study the in-vitro drug release and ex-vivo skin permeation/deposition of the optimized formulation.
- To assess the antifungal activity of the optimized gel against selected fungal pathogens and compare it with marketed formulations.
- To conduct stability studies of the optimized formulation under accelerated ICH conditions.

4. MATERIALS AND METHOD

Ciclopirox olamine was obtained from Lobware Chemicals, Nashik. Soya lecithin (phospholipid) and propylene glycol (co-solvent/humectant) were procured from Cosmo Chem Laboratories, Pune; Tween 80 (edge activator) from Lab Chem Laboratory, Pune; and cholesterol, Carbopol 934 (gelling/bioadhesive polymer) and triethanolamine (neutralizer) from Moly Chem Pvt. Ltd. Absolute ethanol was obtained from Lab Chem, Latur and methyl paraben (preservative) from Oxford Laboratory Chemicals LLP; distilled water was prepared in-house. All chemicals were of pharmaceutical grade. Principal equipment included a Shimadzu BL-220H balance, magnetic stirrer and probe sonicator (Athena Technology), Perkin Elmer FTIR, Shimadzu UV-1800 spectrophotometer, Lab India pH meter, Remi centrifuge, an in-house Franz diffusion cell, AMETEK Brookfield DV2T+ viscometer, and a Thermolab stability chamber.

Preformulation studies established the identity and key properties of the drug. Organoleptic examination, melting-point determination (capillary method) and a shake-flask solubility study in water, ethanol, methanol, propylene glycol and buffer were performed. A UV spectrophotometric method was developed: the λmax of CPO in methanol was 262 nm, and a calibration curve was constructed over 2–10 µg/mL. Drug–excipient compatibility was assessed by FTIR spectroscopy on the drug, individual excipients, their binary mixtures and the final transethosomes.

The transethosomal formulation was optimized using a three-factor, three-level Box–Behnken design (Design-Expert® v9.0) with response surface methodology. The independent variables were soya lecithin concentration (A, 100–200 mg), ethanol concentration (B, 15–35% v/v) and Tween 80 concentration (C, 0.5–1.5 mL), and the responses were particle size (minimize), drug content (maximize) and entrapment efficiency (maximize). The design generated thirteen experimental runs with a fixed drug load of 1% w/v CPO and 5% w/v propylene glycol.

Transethosomes were prepared by the cold method. Soya lecithin, Tween 80, cholesterol (10 mg) and CPO (100 mg) were dissolved in absolute ethanol and propylene glycol by gentle magnetic stirring (300 rpm, 10 min, 25 ± 2 °C) to form a clear organic phase. Distilled water (25 °C) was added dropwise (≈1 mL/min) under continuous stirring at 500 rpm, allowing spontaneous vesicle formation as the ethanol was diluted. The dispersion was probe-sonicated (40 W, 30% amplitude, 10 s on/5 s off, 5 min) to a target size of 100–300 nm and stored in amber vials at 4 °C.

Figure 1: Schematic representation of the cold method for preparation of ciclopirox olamine-loaded transethosomes.

Each batch was characterized for appearance, pH (target 5.5–7.0), and vesicle morphology by optical microscopy. Drug content was assayed spectrophotometrically at 303 nm after disrupting vesicles in ethanol, and entrapment efficiency (EE%) was determined by the indirect ultracentrifugation method (15,000 rpm, 45 min, 4 °C) from the free drug in the supernatant. Particle size and PDI were measured by dynamic light scattering and zeta potential by electrophoretic light scattering. The optimized batch was further examined by scanning electron microscopy (gold-sputtered, 15–20 kV) and X-ray diffraction (Cu Kα, λ = 1.54 Å). In-vitro release was studied in a Franz cell (PBS pH 6.8, 32 °C) over 24 h, and short-term stability was monitored at 0, 1, 2 and 3 months per ICH Q1A(R2).

The optimized dispersion was incorporated into a bioadhesive gel by sprinkling Carbopol 934 (0.5% w/w) onto the dispersion and allowing 2 h hydration; methyl paraben (0.1%) and propylene glycol (5%) were added, and the pH was adjusted to 6.0 ± 0.5 with triethanolamine to induce gelation, with water q.s. to 100 g. Mild mixing at room temperature preserved vesicle integrity. The gel was evaluated for appearance, homogeneity, pH, viscosity (Brookfield), spreadability, drug content and EE%, in-vitro release through cellulose acetate membrane, and ex-vivo permeation through excised goat skin in a Franz cell. Antifungal activity was assessed by the agar well-diffusion method (CLSI M44-A2) against Trichophyton rubrum and Candida albicans, with miconazole and a marketed cream as comparators and DMSO as negative control, and the MIC was determined by broth microdilution. Thermodynamic stability (heating–cooling, centrifugation, freeze–thaw) and accelerated ICH stability (40 ± 2 °C/75 ± 5% RH, 3 months) were also evaluated.

5. RESULTS AND OBSERVATION

5.1 Preformulation Studies

Ciclopirox olamine was a white to off-white, practically odourless, free-flowing crystalline powder with an observed

melting point of 146 °C (capillary; n = 3), consistent with the reported range of 144–147 °C, confirming identity and purity. It was non-hygroscopic and compatible with ethanol. The solubility profile is given in Table 1.

Table 1: Solubility Profile of Ciclopirox Olamine in Different Pharmaceutical Solvents

Sr. No.	Solvent	Solubility Classification	Observation / Remarks
1	Water	Slightly soluble	Partial dissolution; slight turbidity on excess addition
2	Ethanol (95% v/v)	Freely soluble	Clear solution; preferred formulation solvent
3	Methanol	Freely soluble	Clear colourless solution; used for UV calibration
4	Propylene glycol	Soluble to freely soluble	Slightly viscous clear solution; suitable co-solvent
5	Buffer	Slightly to moderately soluble	Hazy; less suitable for aqueous formulation

UV scanning of CPO in methanol gave a λmax of 262 nm. A calibration curve over 2–10 µg/mL (Table 2) was linear, with regression equation y = 0.0535x + 0.0021, R^2 = 0.9981 and a near-zero intercept, confirming Beer–Lambert compliance; this equation was used for all subsequent quantification (Figure 2).

Table 2: Absorbance Values for Calibration Curve of Ciclopirox Olamine in Methanol at 262 nm

Concentration (µg/mL)	Absorbance at 262 nm (Mean ± SD)
0 (Blank)	0.0000 ± 0.0000
2	0.1360 ± 0.0021
4	0.2500 ± 0.0018
6	0.3610 ± 0.0024
8	0.4560 ± 0.0019
10	0.5350 ± 0.0022

Figure 2: Calibration curve of ciclopirox olamine in methanol at 262 nm (y = 0.0535x + 0.0021; R^2 = 0.9981).

5.2 FTIR Spectroscopy

FTIR spectra of the drug, soya lecithin, their binary mixture, an overlay, and the final transethosomes were recorded (Figures 7.5–7.9). The drug retained its principal characteristic bands in the binary mixture and the transethosomes, with only minor shifts attributable to physical interaction and hydrogen bonding, indicating the absence of any major drug–excipient incompatibility. Characteristic interpretations for the drug and the transethosomes are summarized in Tables 3 and 4.

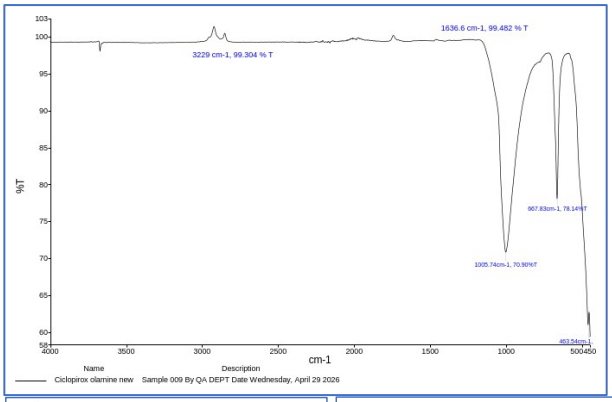

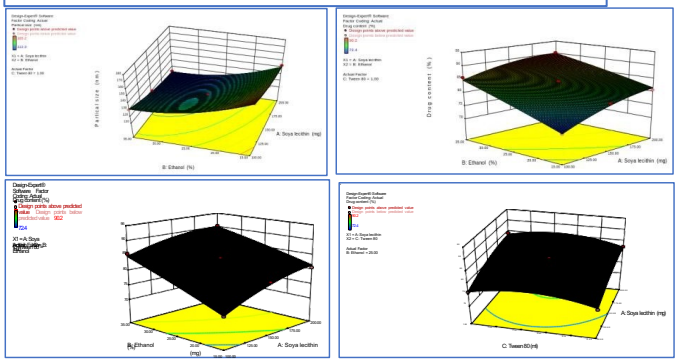

Figure 3 (a, b): FTIR spectra of ciclopirox olamine (left) and soya lecithin (right).

Figure 4 (a, b): FTIR spectra of CPO + soya lecithin binary mixture (left) and overlay of CPO, soya lecithin and Tween 80 (right).

Figure 5: FTIR spectrum of the ciclopirox olamine-loaded transethosomes.

Table 3: Interpretation of Ciclopirox Olamine FTIR Spectrum

Functional Group	Observed Peak (cm^{-1})	Standard Range (cm^{-1})
O–H / N–H stretching	3229	3200–3400
C=O / aromatic C=C stretching	1636.6	1600–1650
C–O stretching	1005.74	1000–1100
Functional Group	**Observed Peak (cm^{-1})**	**Standard Range (cm^{-1})**
C–H out-of-plane bending	667.83	650–700
Ring skeletal vibration	463.54	450–550

Table 4: Interpretation of Transethosomes FTIR Spectrum

Functional Group	Observed Peak (cm^{-1})	Standard Range (cm^{-1})
O–H stretching	3339.52	3200–3400
C=O / C=C stretching	1637.14	1600–1650
CH_3 bending	1381.57	1360–1390
P–O–C stretching	1137.23	1100–1150
P–O stretching	1042.68	1020–1085

5.3 Optimization by Box–Behnken Design

The thirteen design runs with their observed responses are presented in Table 5. Quadratic models provided the best fit for all three responses, with high R^2 values (0.9962, 0.9900 and 0.9858 for particle size, drug content and entrapment efficiency, respectively) and adequate-precision ratios well above 4 (Table 6).

Table 5: Box–Behnken Design Matrix with Observed Responses

Run	A: Soya Lecithin (mg)	B: Ethanol (% v/v)	C: Tween 80 (mL)	Particle Size (nm)	Drug Content (%)	EE (%)
1	200	25	0.5	137.20	82.40	85.20
2	100	25	0.5	160.30	74.60	76.40
3	200	25	1.5	129.80	84.20	87.10
4	100	25	1.5	154.50	76.30	78.20
5	150	15	1.0	149.40	79.10	81.30
6	150	35	1.0	118.60	88.30	90.40
7	100	15	1.0	165.20	72.40	74.50
8	200	15	1.0	143.10	80.60	83.20
9	100	35	1.0	130.40	85.70	88.10
10 ★	200	35	1.0	112.30	90.20	92.50
11	150	25	1.0	112.30	84.00	85.40
12	150	15	0.5	152.60	77.80	79.90
13	150	35	0.5	121.40	87.20	89.60

Table 6: Goodness-of-Fit Summary for Selected Quadratic Models

Response	Model	Std. Dev.	R^2	Adj. R^2	Pred. R^2	Adeq. Precision
Particle Size (nm)	Quadratic	1.71	0.9962	0.9895	0.9252	38.099
Drug Content (%)	Quadratic	0.88	0.9900	0.9720	0.8270	24.351
Entrapment Efficiency (%)	Quadratic	1.06	0.9858	0.9602	0.7368	20.840

Both soya lecithin (A) and ethanol (B) were highly significant for all responses, higher levels reducing particle size while increasing drug content and entrapment efficiency; Tween 80 (C) had a smaller, significant effect on particle size only. The consolidated linear coefficients are given in Table 7, and the three-dimensional response surfaces in Figure 6.

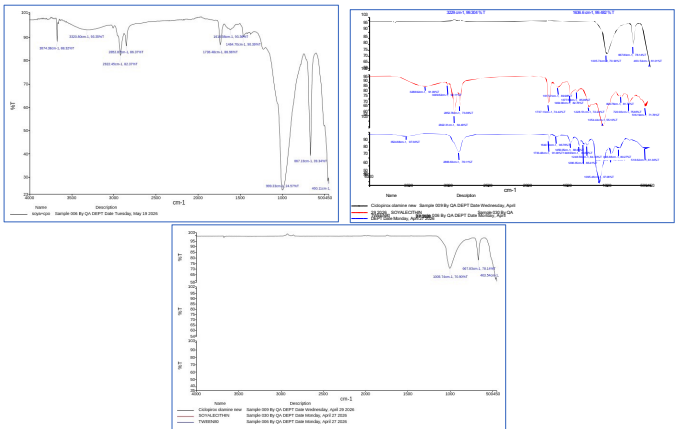

able 7: Consolidated Linear Effect Coefficients and Significance Levels

Response	Intercept	A (p)	B (p)	C (p)
Particle Size (nm)	112.30	11.00 (<0.0001)	15.64 (<0.0001)	2.65 (0.0150)
Drug Content (%)	84.00	+3.55 (<0.0001)	+5.17 (<0.0001)	+0.61 (0.1645)
Entrapment Efficiency (%)	85.40	+3.85 (0.0001)	+5.15 (<0.0001)	+0.65 (0.2091)

Figure 6 (a–c): Three-dimensional response surface plots for particle size (a), drug content (b) and entrapment efficiency (c).

Desirability-function optimization simultaneously targeting minimum particle size and maximum drug content and entrapment efficiency identified the optimized formulation Trans-01 (soya lecithin 200 mg, ethanol 35% v/v, Tween 80 1.0 mL) with a composite desirabilit[illegible] 8). Checkpoint analysis showed excell[illegible]tween predicted and observed responses [illegible]).

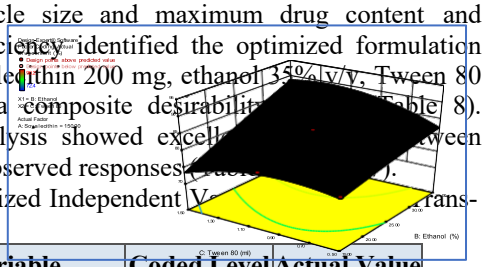

Table 8: Optimized Independent V[illegible]rans-01

Variable	Coded Level	Actual Value
A: Soya Lecithin	+1	200 mg
B: Ethanol	+1	35% v/v
C: Tween 80	0	1.0 mL

Table 9: Checkpoint Analysis Observed vs. Predicted Responses for Trans-01

Response	Predicted	Observed	Residual
Particle Size (nm)	112.30	112.30	0.00
Drug Content (%)	90.20	90.20	0.00
Entrapment Efficiency (%)	92.50	92.50	0.00

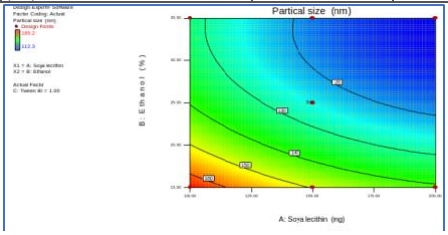

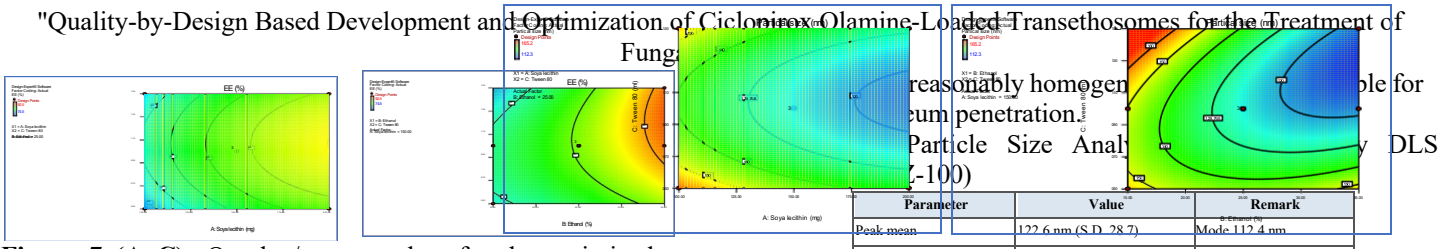

Figure 7 (A–C): Overlay/contour plots for the optimized formulation Trans-01 (A) particle size, (B) drug content and (C) entrapment efficiency (composite desirability, D = 1.0).

5.4 Evaluation of All Batches

All thirteen formulation batches (FB-1 to FB-13) appeared as uniform, pale-to-light-yellow dispersions on visual inspection (Figure 8). Drug content ranged from 72.4% to 90.2% with pH 5.8–6.3 (Table 10), and entrapment efficiency from 74.5% to 92.5% (Table 11); both maxima corresponded to the optimized batch (Figures 9 and 10).

Figure 8: Physical appearance of the thirteen prepared formulation batches (FB-1 to FB-13).

Table 10: % Drug Content and pH of All Batches

Run	% Drug Content	pH	Run	% Drug Content	pH
1	82.40	6.1	8	80.60	6.0
2	74.60	5.8	9	85.70	6.2
3	84.20	6.1	10	90.20	6.3
4	76.30	5.9	11	84.00	6.1
5	79.10	6.0	12	77.80	5.9
6	88.30	6.3	13	87.20	6.2
7	72.40	5.8			

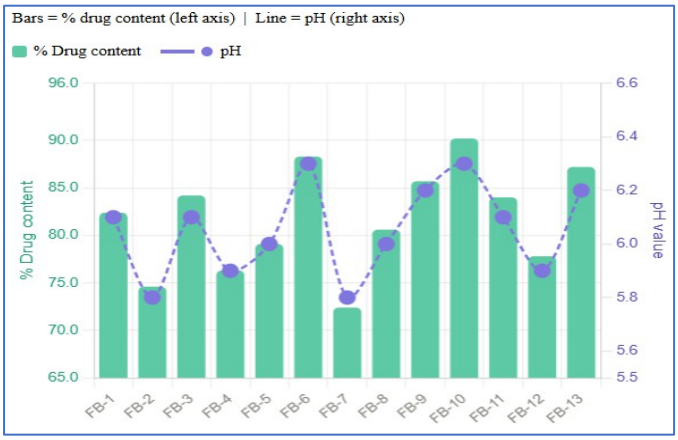

Figure 9: Drug content and pH of all batches.

Table 11: % Entrapment Efficiency of All Batches

Formulation	EE (%)	Formulation	EE (%)	Formulation	EE (%)
F1	85.20	F6	90.40	F11	85.40
F2	76.40	F7	74.50	F12	79.90
F3	87.10	F8	83.20	F13	89.60
F4	78.20	F9	88.10		
F5	81.30	F10	92.50		

Figure 10: Entrapment efficiency (%) of all batches.

5.5 Characterization of the Optimized Formulation (Trans-01)

Trans-01 exhibited a unimodal particle-size distribution with a peak mean of 122.6 nm and a Z-average of 112.30 nm (Table 12, Figure 11). The PDI of 0.353 lies within the acceptable moderate-distribution range (0.3–0.5),

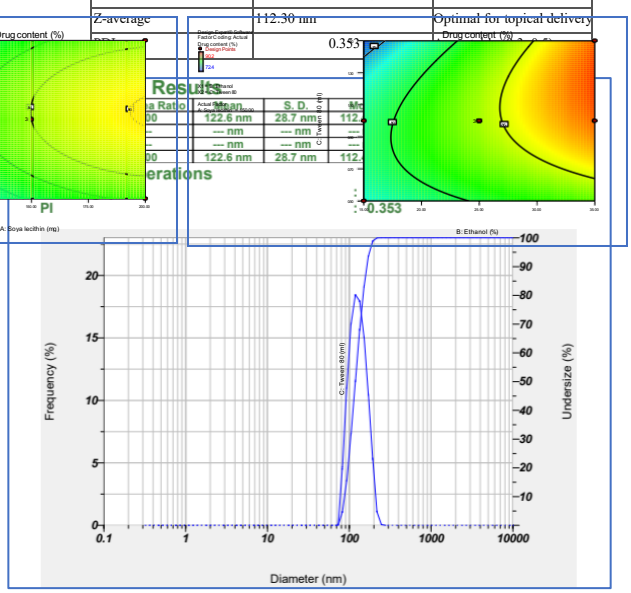

Figure 11: Particle-size distribution profile of Trans-01 (HORIBA SZ-100).

The zeta potential of Trans-01 was 29.7 mV (Table 13, Figure 12), indicating a negative surface charge and moderate-to-good colloidal stability with sufficient electrostatic repulsion to resist aggregation.

Table 13: Zeta Potential Analysis of Trans-01 (HORIBA SZ-100)

Parameter	Value	Implication
Zeta potential (mean)	29.7 mV	Moderate-to-good colloidal stability
Electrophoretic mobility	0.000152 cm²/Vs	Confirmed negative surface charge
Conductivity / Temp.	0.193 mS/cm / 24.9 °C	Low ionic strength; near-physiological

Figure 12: Zeta potential distribution curve of Trans-01.

SEM examination at multiple magnifications (Figure 13) showed discrete, predominantly spherical vesicles with smooth surfaces and well-defined contours. Six measurements on the annotated ×20,000 micrograph gave a mean size of 160.2 ± 25.4 nm (Table 14), broadly consistent with the DLS data.

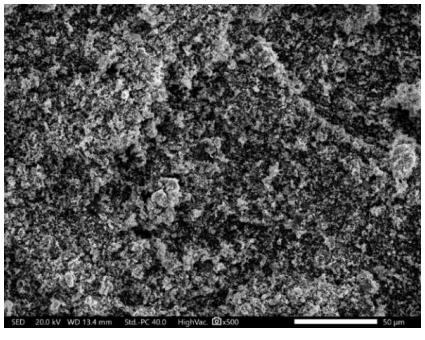

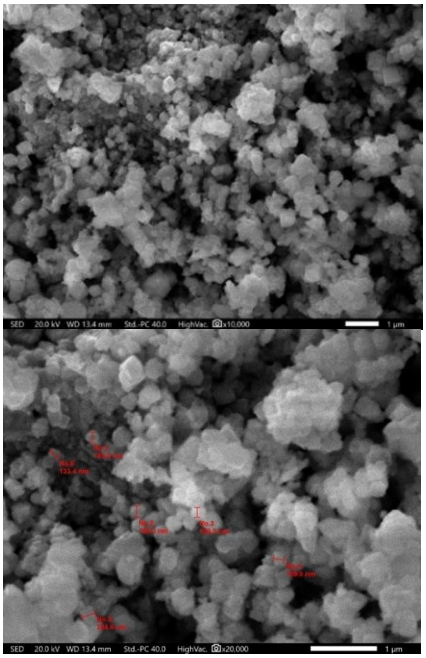

Figure 13 (a–c): SEM micrographs of Trans-01 at ×500, ×10,000 and annotated ×20,000.

Table 14: SEM Particle Size Measurements (Annotated Micrograph, Figure 13c)

No.	Size (nm)	Morphological Feature
1	145.5	Spherical, well-defined contour
2	168.3	Spherical, smooth surface
3	150.5	Spherical, regular boundaries
4	159.0	Spherical, compact structure
5	204.6	Larger aggregated cluster
6	133.4	Spherical, smaller dimension
Mean ± SD	160.2 ± 25.4 nm	

The XRD diffractogram of Trans-01 (Figure 14) was dominated by a broad amorphous halo between approximately 10° and 30° 2θ with only weak superimposed crystalline peaks, indicating that the drug existed largely in a molecularly dispersed or amorphous state within the lipid bilayer (Table 15). This amorphization is consistent with the high entrapment efficiency and predicts improved dissolution and topical bioavailability.

Figure 14: X-ray diffractogram of Trans-01 (Cu Kα, λ = 1.5406 Å), showing a predominantly amorphous halo.

Table 15: XRD Diffractogram Interpretation Trans-01

Parameter	Observation
2θ range / radiation	5–90°; Cu Kα (1.5406 Å)
Predominant pattern	Broad amorphous halo (10–30° 2θ)
Superimposed features	Weak crystalline peaks (~20–30° 2θ)
Material character	Predominantly amorphous with minor crystalline domains
Implication	Successful encapsulation; enhanced dissolution expected

5.6 Evaluation of the Transethosomal Bioadhesive Gel

The optimized vesicles were incorporated into a Carbopol 934 bioadhesive gel (Gel-01), which appeared white to off-white, smooth and homogeneous without phase separation.

Table 16: Evaluation of Transethosomal Bioadhesive Gel Batches

Batch	Appearance	pH	Viscosity (cP)	Spreadability (g·cm/s)	Drug Content (%)
G1	White to off-white	6.3	24,850	6.42	84.85
G2	White to off-white	6.2	31,420	7.86	88.63
G3	White to off-white	5.9	38,760	5.94	90.27

Figure 15: Physical appearance of the developed transethosomal bioadhesive gel.

5.7 In-Vitro Release and Ex-Vivo Permeation

In-vitro release of the transethosomal gel was sustained and markedly higher than the conventional gel, reaching 91.42 ± 1.18% over 8 h versus 38.88 ± 0.94% (Table 17). Ex-vivo permeation through goat skin (Table 18) showed a biphasic profile early diffusion (0–4 h), steady-state flux (4–10 h) and a sustained-release plateau culminating in 66% cumulative permeation at 24 h, reflecting the deformable vesicles' penetration combined with the bioadhesive matrix controlling release (Figure 16).

Table 17: In-Vitro Drug Release Trans-01 vs. Conventional Gel

Time (h)	Trans-01 Cumulative % (± SD)	Conventional Gel Cumulative % (± SD)
0	0.00 ± 0.00	0.00 ± 0.00
0.5	26.25 ± 0.58	3.69 ± 0.42
1	35.86 ± 0.72	7.17 ± 0.55
2	48.99 ± 0.85	13.51 ± 0.68
4	66.92 ± 1.02	24.09 ± 0.80
6	80.32 ± 1.10	32.38 ± 0.88
8	91.42 ± 1.18	38.88 ± 0.94

Table 18: Ex-Vivo Permeation Data of Gel-01 Across Biological Membrane (pH 7.4)

Time (h)	Cumulative Permeation (%)	Phase
0	0	Baseline
2	15	Early diffusion
4	28	Early diffusion
6	40	Steady-state
8	51	Steady-state
10	60	Steady-state
12	63	Sustained release
16	64	Sustained release
20	65	Sustained release
24	66	Plateau

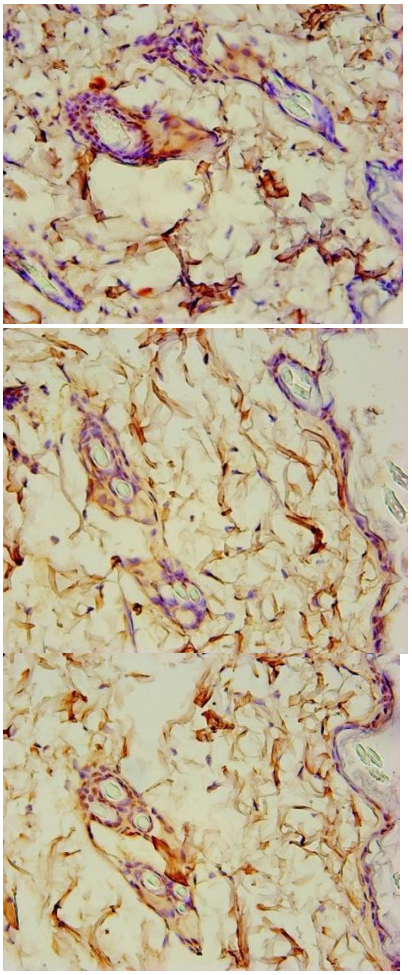

Figure 16: Skin-tissue photomicrographs (400×) after ex-vivo permeation: (A) epidermal penetration, (B) transfollicular deposition, (C) deeper dermal diffusion.

5.8 Antifungal Activity

Against Trichophyton rubrum (ATCC 28188), Gel-01 produced a 14 mm zone of inhibition versus 20 mm for miconazole (1 mg/mL) and 0 mm for the DMSO control (Table 19, Figure 17), confirming that the activity was attributable specifically to the released ciclopirox olamine and equivalent to 70% of the standard. In a comparative study, Gel-01 (16 mm) was comparable to the marketed Candid cream (18 mm), with the blank gel inactive (Table 20, Figure 18).

Table 19: Antifungal Activity of Gel-01 Against T. rubrum (Well Diffusion)

Sample	Zone of Inhibition (mm)	Interpretation
DMSO (negative control)	0	No activity; solvent inactive
Miconazole 1 mg/mL (positive control)	20	Reference standard activity
Gel-01 (transethosomal gel)	14	Significant activity (70% of standard)

Figure 17: Agar well-diffusion plate showing zones of inhibition (DMSO, miconazole, Gel-01) against T. rubrum.

Table 20: Comparative Zone of Inhibition TBG-1 vs. Marketed Formulation

Sample	Zone of Inhibition (mm)	Interpretation
Control (blank gel)	0	No activity; confirms absence of active drug
Marketed (Candid cream)	18	Standard activity against T. rubrum
TBG-1 (transethosomal gel)	16	Comparable to marketed formulation

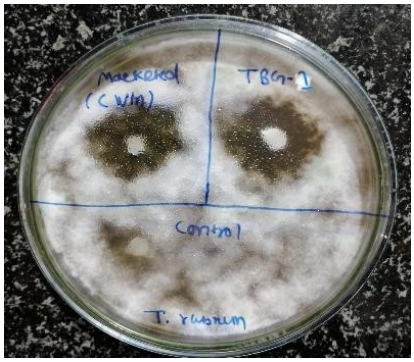

Figure 18: Comparative antifungal study of TBG-1 with the marketed formulation.

5.9 Stability Study

Under accelerated ICH conditions (40 ± 2 °C / 75 ± 5% RH, 3 months), Gel-01 showed no significant change in appearance, pH, viscosity, spreadability, drug content, entrapment efficiency,confirming formulation stability (Table 21).

Table 21: Accelerated Stability Study of Gel-01 (40 ± 2 °C / 75 ± 5% RH)

Parameter	0 Month	1 Month	2 Months	3 Months
Appearance	White	No change	Off-white	Off-white
pH	6.3	6.3	6.2	6.1
Viscosity (cP)	38,760	38,410	38,050	37,680
Spreadability (g·cm/s)	5.94	5.91	5.88	5.85
Drug content (%)	90.27	89.64	89.02	88.65
Entrapment efficiency (%)	92.50	91.88	91.20	90.80
In-vitro release (% / 8 h)	91.42	90.80	90.15	89.60

6. CONCLUSION

A ciclopirox olamine-loaded transethosomal bioadhesive gel was successfully developed using a quality-by-design approach. Preformulation studies confirmed the identity and key physicochemical properties of the drug and a validated UV method at 262 nm, while FTIR ruled out major drug–excipient incompatibility. Transethosomes prepared by the cold method were optimized by a Box–Behnken design, with soya lecithin and ethanol concentrations emerging as the most influential factors; the optimized formulation Trans-01 achieved a particle size of about 112 nm, an acceptable PDI, a moderately negative zeta potential (29.7 mV), and high drug content

(90.2%) and entrapment efficiency (92.5%), with close agreement between predicted and observed responses.

Scanning electron microscopy confirmed spherical vesicles and X-ray diffraction indicated drug amorphization within the bilayer. Incorporation into a Carbopol 934 bioadhesive gel produced a formulation with skin-compatible pH, suitable viscosity and spreadability, sustained in-vitro release (91.4% over 8 h), and biphasic ex-vivo permeation reaching 66% over 24 h. The gel retained meaningful antifungal activity against Trichophyton rubrum, comparable to a marketed product, and remained stable under accelerated ICH conditions.

Overall, the transethosomal carrier offers a rational means of overcoming the penetration limitations of conventional topical antifungal therapy, while the bioadhesive gel base provides a practical, patient-acceptable dosage form for sustained cutaneous delivery. The developed formulation is a promising candidate for the topical management of dermatophytic and candidal skin infections. Future work should extend to skin-irritation and biocompatibility studies, in-vivo efficacy assessment, and long-term stability monitoring to establish clinical translatability.

7. REFERENCES

1. Opatha SAT, Titapiwatanakun V, Chutoprapat R. Transethosomes: a promising nanocarrier for enhanced transdermal drug delivery. Pharmaceutics. 2020;12(9):855.
2. Ascenso A, Raposo S, Batista C, et al. Development, characterization and skin delivery studies of related ultradeformable vesicles: transfersomes, ethosomes and transethosomes. Int J Nanomedicine. 2015;10:5837–5851.
3. Abdulbaqi IM, Darwis Y, Khan NAK, Assi RA, Khan AA. Ethosomal nanocarriers: the impact of constituents and formulation techniques on ethosomal properties, in-vitro studies and clinical trials. Int J Nanomedicine. 2016;11:5023–5040.
4. Bangham AD, Standish MM, Watkins JC. Diffusion of univalent ions across the lamellae of swollen phospholipids. J Mol Biol. 1965;13(1):238–252.
5. Akbarzadeh A, Rezaei-Sadabady R, Davaran S, et al. Liposome: classification, preparation and applications. Nanoscale Res Lett. 2013;8(1):102.
6. Natsheh H, Touitou E. Phospholipid vesicles for dermal/transdermal and nasal administration of active molecules: the effect of surfactants and alcohols on bilayer fluidity and penetration enhancement. Molecules. 2020;25(13):2959.
7. Song CK, Balakrishnan P, Shim CK, Chung SJ, Chong S, Kim DD. A novel vesicular carrier, transethosome, for enhanced skin delivery of voriconazole: characterization and in-vitro/ex-vivo evaluation. Colloids Surf B Biointerfaces. 2012;92:299–304.
8. Ahad A, Raish M, Al-Jenoobi FI, Al-Mohizea AM. Enhanced anti-inflammatory activity of Carbopol-loaded meloxicam transethosomal gel: an ex-vivo, in-vitro study. Drug Deliv. 2020;27(1):446–455.
9. Garg V, Singh H, Bhatia A, et al. Systematic development of transethosomal gel system of piroxicam: formulation optimization, in-vitro evaluation and ex-vivo assessment. AAPS PharmSciTech. 2017;18(1):58–71.
10. Moolakkadath T, Aqil M, Ahad A, et al. Development of transethosomes formulation for dermal fisetin delivery: Box–Behnken design, optimization, in-vitro skin permeation and dermatokinetic studies. Artif Cells Nanomed Biotechnol. 2018;46(8):1783–1794.
11. Natarajan N, David LM, Rangaraj N. Preparation and characterization of ketoconazole transethosomes. J Pharm Res. 2014;8(4):564–570.
12. Brown GD, Denning DW, Gow NAR, et al. Hidden killers: human fungal infections. Sci Transl Med. 2012;4(165):165rv13.
13. Havlickova B, Czaika VA, Friedrich M. Epidemiological trends in skin mycoses worldwide. Mycoses. 2008;51(Suppl 4):2–15.
14. Hay RJ. Dermatophytosis and other superficial mycoses. Cold Spring Harb Perspect Med. 2017;7(8):a026344.
15. Gupta AK, Foley KA, Versteeg SG. New antifungal agents and new formulations against dermatophytes. Mycopathologia. 2017;182(1–2):127–141.
16. Campoy S, Adrio JL. Antifungals. Biochem Pharmacol. 2017;133:86–96.
17. Prausnitz MR, Langer R. Transdermal drug delivery. Nat Biotechnol. 2008;26(11):1261–1268.
18. Bouwstra JA, Ponec M. The skin barrier in healthy and diseased state. Biochim Biophys Acta Biomembr. 2006;1758(12):2080–2095.
19. Jain S, Patel N, Madan P, Lin S. Formulation and rheological evaluation of ethosome-based topical gel of voriconazole for the treatment of cutaneous fungal infections. Eur J Pharm Biopharm. 2017;119:1–12.
20. Chen M, Liu X, Fahr A. Skin delivery of ferulic acid from different vesicular systems. J Biomed Nanotechnol. 2010;6(6):768–775.